Advanced Materials

～夢をかたちに～

新素材

CRDAM Newsletter

共同研究開発センター

Vol.8
2016.12

CONTENTS

東北大学　金属材料研究所　附属新素材共同研究開発センター
Cooperative Research and Development Center for Advanced Materials, IMR, Tohoku University

第132回 東北大学 金属材料研究所講演会

とき：2016年11月24(木)～25日(金)
ところ：金属材料研究所2号館講堂

「環境浄化ならびに骨伝導性に優れたTiO_2の研究」

教授 正橋 直哉

第132回所内講演会の二日目に「環境浄化ならびに骨伝導性に優れたTiO_2の研究」と題する講演を行いました。本講ではTiやTi基板上にTiO_2を形成するにあたり、陽極酸化法を採用しました。電解浴組成や化成電圧等の電気化学条件を制御することで、TiO_2の多孔質化やアニオンドープによるバンド構造改質が可能となり、触媒活性の向上や可視光応答性の改善の結果、脱臭性や抗菌性が発現することを紹介しました。さらに、本所で開発した低ヤング率と高強度を備え、生体適合性に優れたTiNbSn合金基板に陽極酸化TiO_2を生成し、温水処理後にin vitro試験により骨伝導性を調査した結果、ハイドロキシアパタイトの生成を確認しました。この陽極酸化材を日本白色家兎にインプラント（in vivo試験）したところ、骨との密着強度は陽極酸化を施していない試料より高く、骨の構成元素であるCaやPのTiO_2への浸透を確認しました。本法で創製した陽極酸化TiO_2は光触媒機能を有することから、インプラント前に紫外線照射による殺菌が可能であり、力学的性質を損なうことなく生体内で骨伝導性を確保できると考えられます。また、骨伝導性を高めるには結晶性の高いTiO_2の基板担持が有効で、陽極酸化時の電気化学条件の選択が重要であると提案しました。講演後、数件の質問を頂き、活発な討議を行うことができました。

構造用材料としてのTiO_2を説明する正橋教授

「機能性ホイスラー合金の磁気特性と電子状態」

准教授 梅津 理恵

「機能性ホイスラー合金の磁気特性と電子状態」という題目にて第132回金研講演会にて研究紹介を行いました。多種多様なホイスラー合金の中でも、3d遷移金属元素が磁性の主役を担う物質に興味を持っており、「ハーフメタル」という特異な電子状態を有するCo基、Mn基ホイスラー合金の相安定性、結晶の規則度と磁性や電子状態との関連性、そして、最近行った、磁場中共鳴非弾性X散乱測定によって得られた結果を紹介しました。

ホイスラー合金において、電子状態と原子の規則配列は密接に関連しており、規則度を精密に評価するために中性子回折実験を行い、磁気構造や磁気モーメントの大きさ等も併せて調べました。また、原子の配列を制御した物質において、「本当に」ハーフメタル型の電子状態を有しているかを検証するために種々の物性測定を行ってきました。SPring-8のBL07LSUではフェルミ面近傍のd-d励起に関与する非弾性散乱スペクトルの円偏光依存性を調べ、電子状態密度がアップスピン・ダウンスピンサイトで大きく偏っていることを示唆する結果も得られました。

今後も、ホイスラー合金の電子状態と磁性に関する一連の研究を行っていくと共に、新規機能性を有する物質の探索も行っていきたいと考えております。新素材センターでは、試料の作製から基本的な性質の評価に至るまで、あらゆる場面で日頃よりお世話になっております。今後ともどうか宜しくお願い致します。

ホイスラー合金の構成元素について説明する梅津准教授

体験実験

東桜学館高等学校の 1 年生 7 名が当センターで体験実験を行いました

平成 28 年 10 月 5 日(水)に山形県立東桜学館高等学校より、1 年生男女 29 名が「きんけん体験学習(アカデミックツアー)」に参加するため本所を訪れました。そのうちの 7 名が、梅津准教授・張助教の指導のもと、「金属材料の原子の規則配列と磁気状態」のテーマにて体験実験を行いました。当センターのアーク溶解炉、メルトスパン装置、X 線解析装置等を使い、もともと磁石につかない元素同士でも合金化することで、突然磁石に反応するような性質を示したり、同じ材料でも結晶構造や原子の配列が変わることで磁石に反応する強さが変わることを実験を通して体験し、その理由を考えたりしました。1 日がかりのツアーでしたが、最後まで集中して取り組んでいました。

体験後のアンケートでは「普段ではできないような貴重な体験が出来た。」、「初めて見るような機会がたくさんあり、一つの性質の違いを出すためにも目的に応じて幾つもの装置があることを知った。」、「自分の知りたい疑問だけでなく、発展的な事も教えてもらって勉強になった。」等たくさんの感想が寄せられました。また、意見欄では「どんな金属でも混ぜ合わせることはできるのか？」、「勉強や研究などにやる気を出す方法は？」などユニークな質問もありました。

真剣に覗き込む学生

メルトスパンで作製した試料を取り出すところ

見学

八戸北高等学校の 1 年生 30 名が当センターを見学しました

平成 28 年 8 月 4 日(木)に青森県教育委員会「平成 28 年度あおもりグローバルスチューデント育成事業」のもと、青森県立八戸北高校から 1 年生 40 名が研究所見学のため来所しました。4 つのグループに分かれ、所内の研究室やセンターなど 3 ヵ所を見学しました。当センターもルートとなり、3 つのグループ、計 30 名が訪問しました。各グループにつき約 30 分と短い時間ではありましたが、梅津准教授が対応し、当センターの概要パンフレットを配布して説明した後、センターの設備として「アーク室」、「単結晶化室」、「X 線室」、「表面分析室」などを紹介しました。

センター長室にてセンターの概要を説明中

X 線室にて実験の様子を見学中

平成 28 年度客員教員(国外)成果報告

Extremely quantum confined electronic energy spectrum and optical properties of ultra-stable CdSe and ZnO nano-clusters

Prof. Igor Dmitruk
National Taras Shevchenko University of Kyiv, Ukraine

From 1st of July to 31st of August 2016 I worked as a visiting professor in the Cooperative Research and Development Center for Advanced Materials at the Institute of Materials Research, Tohoku University working with Associate Professor Rodion Belosludov. During this visit I have worked on the problem of structure determination of ultra-stable CdSe and ZnO nanoclusters having extremely small size and their possible role as seeds for zinc oxide tetrapods grows.

Zinc oxide is a promising material for applications in photonics and optoelectronics. It has advantages of wide direct bandgap, stability, and it consists of very abandoned atoms. Not less important is the fact that zinc oxide is nontoxic and environment friendly. Zinc oxide nanoparticles have additional advantages of structure variations and tuning of electronic energy bands.

Recently we have found a novel series of magic nanoclusters $(AB)_n$ for II-VI compounds with n = 13, 19, 33, 34, and 48. For the case of CdSe $(CdSe)_{33}$ and $(CdSe)_{34}$ magic nanoclusters have been prepared in macroscopic quantities. However, ZnO demonstrate formation of another series of magic nanoclusters $(ZnO)_n$ with n = 12, 34, 60, 78, and 168 (Figure 1). Only one magic number n = 34 is the same for ZnO and other studied II-VI compounds. Theoretically, the structure of $(CdSe)_{34}$ originally proposed is a core-cage arrangement in which core of $(CdSe)_6$ is contained in the empty cage $(CdSe)_{28}$, denoted as $(CdSe)_{28}(28+0)$, to form $(CdSe)_{34}(28+6)$. The empty cage $(CdSe)_{28}(28+0)$ is basically a polyhedral atomic shell consisting of 24 six-member-rings of alternating -Cd-Se- network with 6 four-member-rings which bend the shell to smoothly close the network as a hollow cage. Probably nanocluster $(ZnO)_{34}$ has the same structure. To reveal the structure of others we should notice that the series of $(ZnO)_n$ magic nanoclusters starts with n=12 which is well-known magic number for binary fullerenes corresponding to the smallest closed shell with isolated squares. To check its stability for ZnO we have performed the first-principles calculations on HITACHI SR16000-M1 supercomputer.

Full geometry optimization and vibrational and electronic spectra analyses of ZnO nanoclusters have been performed using density functional theory (DFT) with B3LYP exchange correlation functional and 6-31G basis set. Time-dependent DFT (TDDFT) has been applied for electronic excited states calculations.

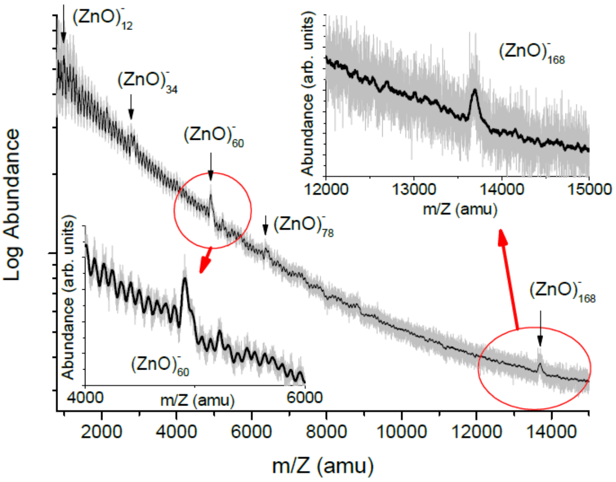

Figure 1. The time-of-flight mass spectrum of zinc oxide clusters obtained by laser ablation of zinc peroxide powder. Gray line displays measured signal, black line shows the smoothed spectrum. The clusters of enhanced stability are pointed and labeled. Insets show the fragments of the spectrum in the vicinity of $(ZnO)_{60}$ and $(ZnO)_{168}$ cluster mass regions in linear scale.

Structure optimization of ZnO nanoclusters with different starting geometries revealed their tendency to form shell structures. For example, Figure 2 shows several steps of optimization of the structure of $(ZnO)_{12}$ nanoparticle starting from wurtzite bulk crystal fragment.

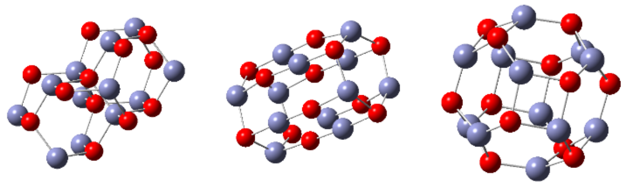

Figure. 2. Gradual structure transformation (from left to right) of $(ZnO)_{12}$ nanoparticle during geometry optimization.

Unlike other II-VI compounds it relaxes spontaneously to closed shell structure. That demonstrates its elevated stability.

Another example is determination of the structure of *n*=34 nanocluster. For CdSe the largest binding energy has core-cage $(CdSe)_{34}(28+6)$. We have performed similar calculations for the different isomers of $(ZnO)_{34}$ nanocluster: core-cage, empty cage, bulk fragment, etc. Surprisingly, the most precise MP2 calculations show that binding energy of core-cage (28+6) and empty cage structures are equal within precision of 0.01 Hartree.

Taking into account this trend of ZnO to form closed shells we can suggest the following structures of magic ZnO nanoclusters observed in mass-spectroscopy. They consist of concentric nested (onion-like) shells of $(ZnO)_{12m^2}$, m=1, 2, 3. The first shell at m=1 is $(ZnO)_{12}$, the second one at m=2 is $(ZnO)_{48}$, the third one at m=3 is $(ZnO)_{108}$. The cluster $(ZnO)_{60}$ consists of the two shells: $(ZnO)_{12}$ inside of $(ZnO)_{48}$. $(ZnO)_{168}$ cluster has three nested shells: $(ZnO)_{12}$, $(ZnO)_{48}$, and $(ZnO)_{108}$ (Figure 3). In this way, the simple mathematical sequence exactly describes the experimentally observed magic numbers is the mass spectra. Following the sequence, the next closed atomic shell ZnO clusters will be $(ZnO)_{360}$, $(ZnO)_{660}$, and so on.

Topologically, the sequence of $(ZnO)_n$, $n = 12m^2$, m = 1, 2, 3 and so on shells can be described as the set of Goldberg polyhedra G(a,b) of octahedral symmetry with tetragons instead of pentagons and a = b: $G_{IV}(1,1)$, $G_{IV}(2,2)$, $G_{IV}(3,3)$ and so on. Unlike carbon, for describing the shells of which the polyhedra were successfully applied, Zinc and Oxygen atoms alternate in vertices of both tetragons and hexagons, so each the atom has three neighbors of the other element, and the octahedral symmetry of the polyhedra changes to the tetrahedral one, while the octahedral shape of the polyhedra remains. Of course, as Euler characteristic of a convex polyhedron equals to 2, the Goldberg polyhedra built of tetragons and hexagons have exactly 6 tetragonal faces. The higher stability of the shell is expected for the case of isolated tetragons, and moreover, if they are spread evenly on the polyhedron surface, analogously to isolated pentagon rule for buckminsterfullerene. To support the suggestion of onion-like shell structure of the magic ZnO clusters the first-principles calculations have been performed. The structures of $(ZnO)_{12}$, $(ZnO)_{60}$, $(ZnO)_{168}$, and $(ZnO)_{360}$ clusters have been optimized at MP2/6-31G, B3LYP/6-31G, HF/6-31G, and AM1 theory levels, respectively. The highest theory level used for each the cluster was restricted by rational calculation time and the software capabilities.

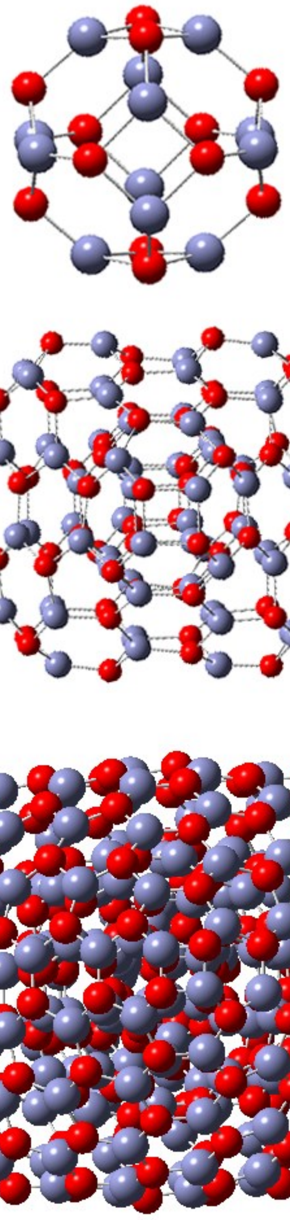

Figure 3. Optimized structure of ZnO nested cages clusters: $(ZnO)_{12}$, $(ZnO)_{60}(48+12)$, and $(ZnO)_{168}(108+48+12)$.

The symmetry group of all the shown nested shell structures is T_h. The stationary points of geometry optimization have been checked to be a minimum by harmonic vibrational frequency analysis. For $(ZnO)_{12}$, all the frequencies are positive, thus, the T_h symmetric shell is indeed the minimum point of potential energy surface. However, “negative” frequencies were found for the T_h symmetric structure of $(ZnO)_{60}$. After decreasing the symmetry down to C_1, applying small random shifts of all the atoms, and optimizing the geometry again, the structure has been adjusted slightly, which has 199 meV lower total energy than the corresponding initial structure, and all the vibrational frequencies positive. The distortion of the initial T_h symmetric nested shell structure is rather small and it can be explained by Jahn-Teller effect.

This symmetry reduction from Th to T point group was observed for studied nested shells ZnO clusters. It should be noted that further symmetry reduction does not increase binding energy indicating that T is the actual point group of these clusters.

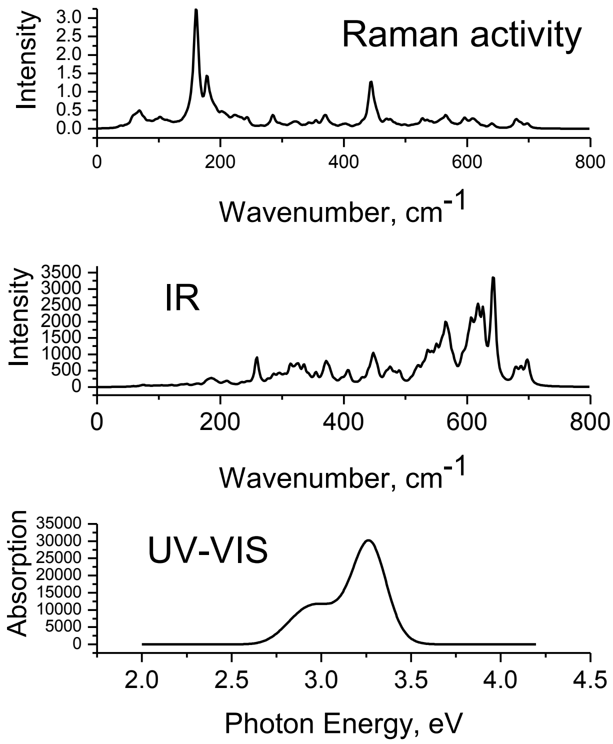

Figure 4. Calculated vibrational and electronic spectra of $(ZnO)_{34}$(28+6) nanocluster.

It is naturally to affiliate seeds of well-known ZnO tetrapods, which have tetrahedral symmetry, with $(ZnO)_{168}$ magic clusters (and, probably, with the larger ones, $(ZnO)_{360}$, $(ZnO)_{660}$, and so on), which have the same T symmetry. Tetrapods, but not T symmetry crystals, grow because faces of the clusters consist of hexagons that are energetically favorable, while vertexes contain squares that are energetically unfavorable.

Although ZnO magic-sized nanoclusters have not been prepared in macroscopic quantity we can study their physical properties theoretically in comparison with CdSe. Figure 4 presents calculated infrared, Raman, and optical absorption spectra of $(ZnO)_{34}$(28+6) nanocluster. Unlike CdSe it shows no gap in vibrational density of states. Active modes are distributed more evenly in the spectrum. On the other hand, electronic spectrum demonstrates more similarity to CdSe. Probably it can attributed to larger ionicity of zinc oxide which leads to difference in interatomic bonds strength and directionality. While electronic spectrum is determined mostly by quantum confinement effect which is similar for clusters of the same size and structure.

Predicted difference in vibrational spectra can be used to distinguish onion-like shell structures predicted for ZnO from less regular core-cage structures like $(CdSe)_{34}$(28+6) which are energy favourable for other II-VI compounds.

These clusters can be used as building blocks of novel nano-devices and nano-composite materials for applications in nano-electronics and photonics.

I appreciate invitation to Tohoku University and this unique chance for fruitful collaboration. Many thanks to Director of IMR Prof. Koki Takanashi, Head of Cooperative Research and Development Center for Advanced Materials Prof. Tadashi Furuhara, and my colleague Assoc. Prof. R. Belosludov. I also thankful to Mr. N. Igarashi for continuous support in computer code and facility and Ms. E. Takahashi in her assistance for my family to stay in Sendai.

ありがとう ございました

平成 28 年度非常勤講師成果報告

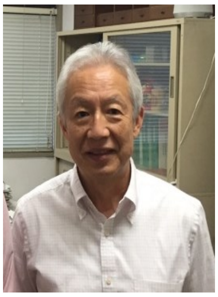

Ultrasonic Materials Processing

Professor Teiichi Ando, Ph.D.
Northeastern University, USA

I was a visiting researcher in the Cooperative Research and Development Center for Advanced Materials, hosted by Professor Hidemi Kato of the Institute of Materials Research for the period from September 5th to 30th. During my short stay in the Kato Lab, I have had opportunities to address my research in ultrasonic materials processing in the form of a seminar and to exchange ideas on non-equilibrium materials processing with Prof. Kato and his colleague Prof. Takeshi Wada. I also had an opportunity to discuss research on droplet-based material processing with Prof. Noriharu Yodoshi of the IMR. The main points of the thoughts communicated to and exchanged with the people I met during my stay at IMR are outlined below.

While there are a variety of methods by which we can create non-equilibrium thermodynamic states in materials, the specific methods I have been investigating are rapid solidification processing and high strain-rate ultrasonic deformation processing. Of the two approaches, my seminar focused on high strain-rate ultrasonic deformation processing. In high strain-rate deformation, as in ultrasonic joining, excess vacancies generated by the non-conservative motion of jogs on screw dislocations remain in the material at a high concentration. An in situ NMR study on deforming pure aluminum [1] has revealed vacancy mole fractions as high as 0.1, Figure 1. High prior vacancy concentrations have also been estimated in aluminum wire subjected to ultrasonic deformation by TEM, Figure 2 [2].

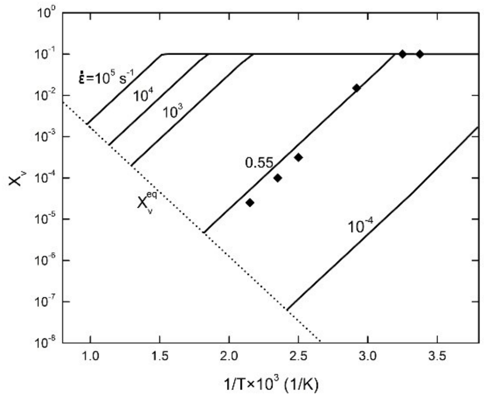

Figure 1: Excess vacancy concentration in deforming pure aluminum; determined by NMR at a strain rate of 0.55 s^{-1} and predicted at various strain rates [1]

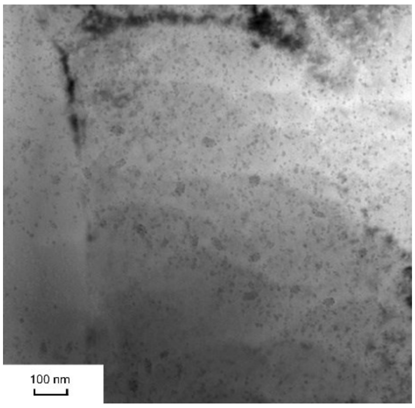

Figure 2: Vacancy clusters and Frank loops in pure aluminum wire subjected to ultrasonic deformation at 773 K for 1 s [2]

Excess vacancies in high concentrations may impact material behavior in three ways; through their effects on diffusion, thermodynamic stability and mechanical behavior. They enhance substitutional diffusion possibly by many orders of magnitude as deduced from the relation $D/D^{norm}=X_V/X_V^{eq}$ where D is the enhanced diffusivity, D^{norm} is the normal diffusivity in the annealed state and X_V^{eq} is the equilibrium concentration of thermal vacancies. This effect was confirmed by ultrasonic diffusion couple experiments of aluminum and copper sheets in which the diffusivity of copper in aluminum was determined to be five orders of magnitude above the normal value calculated at the joining temperature [3].

Excess vacancies would also increase the free energy of the solid in which they are generated, possibly causing melting even below the equilibrium melting point. Figure 4 shows a plot of normalized melting point, $T_M(X_V)/T_M^{eq}$, against X_V where significant melting point depression is predicted when X_V exceeds 0.01. Calculations for other metals, e.g., copper and nickel, also yield similar results.

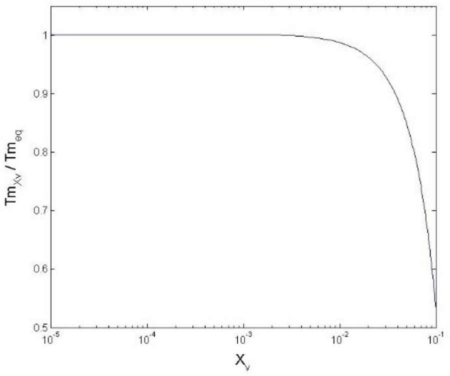

Figure 3: Normalized melting point of aluminum calculated as a function of vacancy concentration [3]

Another important effect of excess vacancies is the osmotic force exerted on dislocations that causes them to climb at high speed. The osmotic climb force on a mixed dislocation, given by [4]

$$F_c^{osm} = \frac{kT}{b^3}\frac{\left(\vec{b}\times\vec{t}\right)\times\vec{t}\cdot\vec{b}}{\left|\left(\vec{b}\times\vec{t}\right)\times\vec{t}\right|}\ln\frac{X_V}{X_V^{eq}} \qquad (1)$$

where $\vec{b}$ is the Burgers vector and $\vec{t}$ is the dislocation line vector, translates into an effective hydrostatic pressure of 600 MPa at a vacancy concentration just 50% above the equilibrium value, and 10,000 MPa when X_V / X_V^{eq} is increased to 10^3, which may readily occur in a metal subjected to ultrasonically deformation. Thus, excess vacancies would accelerate recovery and recrystallization to their highest rates, possibly offsetting the concurrent strain hardening. Such softening in a metal subjected to ultrasonic deformation is seen in Figure 4 where pure aluminum wire subjected to ultrasonic deformation is actually softer than the as-received wire. The occurrence of dynamic recovery and recrystallization was confirmed in aluminum subjected to ultrasonic deformation [5].

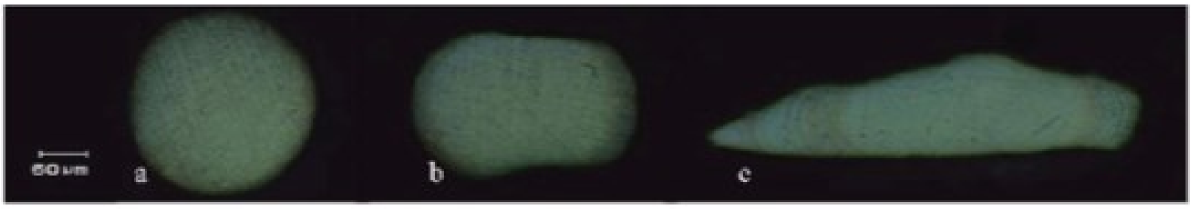

Figure 4: Cross sections and micro-hardness of aluminum wire: (a) as-received, (b) subjected to ultrasonic vibration for 1 s at room temperature under 460 N, (c) subjected to ultrasonic vibration for 1 s at 773 K under 67 N [2].

Ultrasonic powder consolidation (UPC), a new low-temperature powder consolidation technique [6, 7], can produce full-density, metallurgically intact consolidates in seconds, Figure 5. Systematic UPC experiments with copper powder have indicated that the rapid consolidation in UPC occurs by a mechanism that involves the three effects of excess vacancies on diffusion, thermodynamics and dislocation mobility [8].

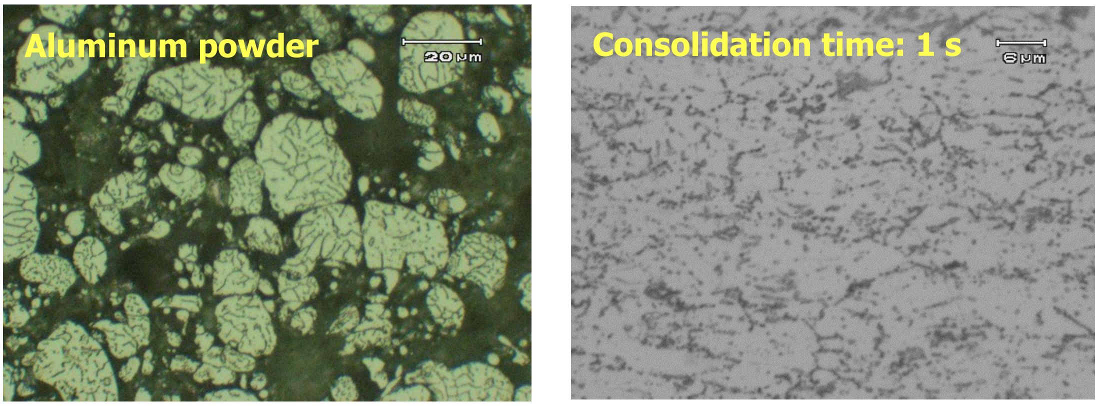

Figure 5: Cross sections of (a) aluminum powder particles and (b) bulk aluminum consolidated from the powder by UPC at 573 K under 100 MPa [6].

Excess Further work is needed to more fully elucidate the effects of ultrasonic deformation processing on material behavior and exploit them in non-equilibrium materials processing. New areas of research that are identified include fabrication of energetic materials, rapid low-temperature material synthesis, simultaneous consolidation and joining of coatings, duplex (multiplex)-structured materials, porous materials, simultaneous mechanical alloying and consolidation, consolidation of amorphous powders, additive manufacturing and fundamental investigation of phase transformations in the presence of crystalline defects. Future collaborations were discussed with the IMR PIs, Profs. Kato and Wada, in the areas of ultrasonic processing of nanoporous materials and amorphous powders.

In closing, I sincerely thank my host Professor Hidemi Kato for inviting me to his lab as a visiting scholar, without which my sabbatical in Japan would not have been so fruitful.

References

[1] K. Murty, K. Detemple, O. Kanert, and J. Th. M. DeHosson: Met. and Mater. Trans. A, vol. 29A, 1998, pp. 153-59.
[2] D. Colanto, PhD thesis, Northeastern University, 2010
[3] T. Hu, S. Zhalehpour, A. Gouldstone, S. Muftu and T. Ando, Metall. Mater. Trans. A, vol. 45A, 2014, pp. 2545-52.
[4] J. P. Hirth and J. Lothe, *Theory of Dislocations*, McGrow-Hill, New York, 1968.
[5] Z. Huang, unpublished work, Northeastern University, 2016.
[6] I.E. Gunduz, PhD thesis, Northeastern University, 2006.
[7] D. Erdeniz and T. Ando, Int. J. Materials Research, vol. 104 (4), 2013, pp. 386-91.
[8] Z. Liu, unpublished work, Northeastern University, 2016

展示室見学･視察一覧

2016/ 7/26	栃木県立宇都宮工業高等学校機械科 2 年生 1 名
2016/ 8/ 4	青森県立八戸北高等学校より 1 年生 40 名(そのうち 30 名が当センターを見学)
2016/10/5	山形県立東桜学館高等学校より 29 名(そのうち 7 名が当センターにて体験実験)

新素材共同研究開発センターニュース Vol.8
2016 年 12 月 5 日
東北大学　金属材料研究所
附属新素材共同研究開発センター
〒980-8577　宮城県仙台市青葉区片平 2-1-1
TEL：022-215-2371／FAX：022-215-2137
E-MAIL：crdam@imr.tohoku.ac.jp
URL：http://www.crdam.imr.tohoku.ac.jp